Discretized Clay Shell Model (DCSM) of Clayey Sandstone: Evaluating the Effective Stress Coefficient of Permeability

P. L. Tai[1], and J. J. Dong[1, 2]

[1]Graduate Institute of Applied Geology, National Central University, Taoyuan 32001, Taiwan

[2]Earthquake-Disaster & Risk Evaluation and Management Center, National Central University, Taoyuan 32001, Taiwan

Corresponding author: Jia-Jyun Dong (jjdong@geo.ncu.edu.tw)

Key Points:

- We proposed Discretized Clay Shell Model (DCSM) to account for the stress dependent elastic modulus of clay.
- The proposed DCSM predicts a pore pressure and confining stress dependent effective stress coefficient.
- The predicted α for soft, high stress dependent deformability of clay coating on the pores of sandstones could be far higher than 1.

Abstract

The effective stress coefficient α determines the effective stress, which dominating the permeability of rocks. However, the documented value of α for rocks shows a high scatter (0.3-5.5), based on the laboratory measurement. The well know Clay Shell Model (CSM) successfully explain why the α of the clayey sandstone can well above 1 theoretically. However, CSM cannot account

for the stress dependency of α observed experimentally. In this study, a modification of CSM was proposed. This proposed Discretized Clay Shell Model (DCSM) discretizing multi-layers clay domain to account for the stress dependent elastic modulus of clay. Response surface method was used to determine the effective stress coefficient α under different combination of confining stress and pore pressure. The parametric study and the prediction of permeability-depth relation using synthetic case illustrate the superior features of the proposed DCSM to the traditional CSM, especially when the clay content is high. Critical findings includes: (1) The predicted effective stress coefficient α form a concaving upward surface in the pore pressure-confining stress space using DCSM even when the material properties of clay and grain remain unchanged. (2) The influence of pore pressure on α (positive correlation) will be stronger than the influence of confining stress especially under low pore pressure. (3) The predicted α is not necessary positively or negatively correlated to confining stress under constant pore pressure. (4) The predicted α for soft, high stress dependent deformability of clay coating on the pores of sandstones could be far higher than 1.

1 Introduction

The stress dependent permeability k of sandstone, one of the important reservoirs, is a key parameter for fossil fuel exploitation (e.g., Li et al., 2008) and carbon geological sequestration (e.g., Cui et al., 2007). The general stress dependency of permeability k can be expressed as $k = f(\sigma_c, P_p)$, where σ_c is confining stress and P_p is pore pressure. This two-variable function can be replaced by a single variable function $k = f(\sigma_{eff})$ if an effective stress principle is valid (e.g.,

Bernabe, 1987; Al-Wardy and Zimmerman, 2004; Li et al., 2009; 2014), where σ_{eff} is the effective stress.

The effective stress dominating the permeability of rocks has been defined by many researchers (e.g., Bernabe, 1987; Berryman, 1992; Al-Wardy and Zimmerman, 2004; Li et al, 2009, 2014) as follows:

$$\sigma_{eff} = \sigma_c - \alpha P_p \quad (1)$$

where α is effective stress coefficient of permeability. This parameter α is a measure of the relative sensitivity of pore pressure and confining pressure to the permeability *k* (Al-Wardy and Zimmerman, 2004). If α is a constant, the effective stress σ_{eff} can easily be determined by σ_c and P_p, separately.

When the confining stress are significantly larger than the pore pressure (e.g., permeability measurement in laboratory under high confining stress), precise determination of the effective stress coefficient α is not critical due to minor contribution of the P_p to effective stress when Eq. (1) was used. However, many sedimentary basins on continental margins hold abnormally high pore pressure at depths (Breckels, 1982; Gaarenstroom et al., 1993; Engelder and Fischer, 1994). The parameter α become critical for predicting the permeability *k* at burial depth. Moreover, the de-pressurization during the production lifecycle of a reservoir changes the pore pressure P_p and the effective stress σ_{eff} can only be evaluated if α can be determined in prior. Although different effective stress dependent relations of permeability are available (e.g., Dong et al., 2010), the prediction of sandstones' permeability at different depths are still challenge, since the comprehension of effective stress coefficient α at different burial depth is limited.

For most of the rocks (e.g., crystalline rocks, clean granular rocks, chalks, shales and so forth), the values of α close to but lower than 1 have been reported (e.g., Berryman, 1992). Some experimental studies found α of clayey sandstone and tight sandstone range in 0.60 to 0.85. (e.g.

Abass et al., 2009). However, Zoback and Byerlee (1975) measured permeability of the clayey Berea sandstone and found the α is ranging from 2.20 to 4.00. This result was supported by other experimental studies such as Walls and Nur (1979). To account for the observations of α larger than 1, Zoback and Byerlee (1975) proposed a conceptual model, Clay Shell Model (CSM). They suggested soft clay coating on wall of grains (e.g., double layers) and the shape of pores is assumed as cylinder. The grains, clay and pores system of clayey sandstones was conceptualized in Fig. 1a.

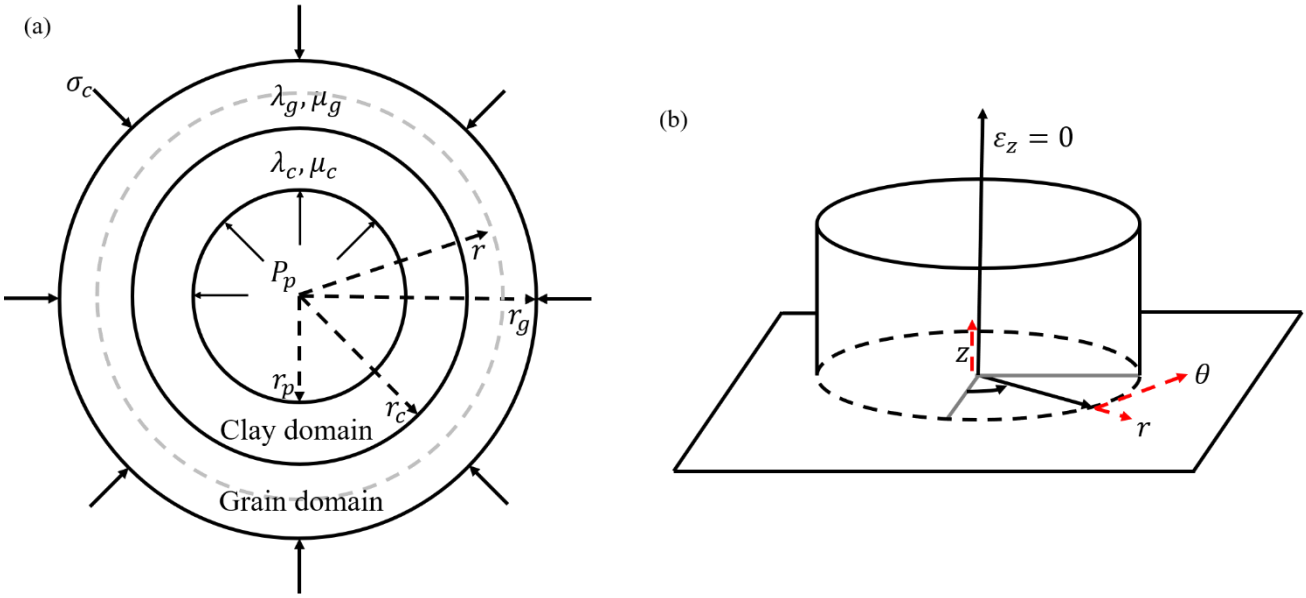

Figure 1. (**a**) Clay Shell Model (CSM, modified from Al-Wardy and Zimmerman, 2004) for clayey sandstone. The clayey sandstone was conceptualized as grains, clay, and pore system; (**b**) Cylinder pore and the plane strain condition (vertical strain (in direction of z axis) equals to zero). The cylindrical polar coordinate was selected.

In Fig. 1a, the r is the radial distance from the center of pore to a specific point within the clay and grain domains. The r_p, r_c and r_g are the pore radius, distance from the center to the inner and outer boundaries of grains, respectively. The domain between r_p and r_c are composed of clay, and

the domain between r_c and r_g are composed of sand grains. The μ_g and μ_c are the shear modulus of sand grain (between r_c and r_g) and clay (between r_p and r_c), respectively. The variation of r_p versus σ_c and P_p determines the effective stress coefficient for deformability and porosity $\phi(=\frac{r_p^2}{r_g^2})$, as well as for the permeability, which will be introduced in more detail later (Section 2.1).

Since the elastic moduli of the clay are usually smaller than the one of grains, the influence of pore pressure on the pore radius should be larger than the influence of confining pressure. That is, this heterogeneity of clayey sandstones resulted in $\alpha > 1$ (Zoback and Byerlee, 1975). Al-Wardy and Zimmerman (2004) elaborated the CSM further following the idea proposed by Zoback and Byerlee (1975). Based on CSM (details will be introduced in Section 2.2), the effective stress coefficient α will be function of shear modulus of grains and clay, as well as the clay fraction F_c defined as follows:

$$F_c = \frac{r_c^2 - r_p^2}{r_g^2 - r_p^2} \tag{2}$$

The derived α is a constant which is irrelevant to the variation of confining stress σ_c and pore pressure P_p, which is contradict to the observations of many previous studies (Todd and Simmons, 1972; Coyner, 1984; Gangi and Carlson, 1996). Notably, the elastic moduli of sand grains and clay (μ_g and μ_c) are assumed as stress independent for the CSM. It is not a realistic for the elastic moduli of sand grains and clay which are stress-dependent (Mondol et el., 2008). Since the α should not be a constant but varied with changing σ_c and P_p, the equation used to calculate the effective stress would be modified slightly from Eq. (1) (e.g. Robin, 1973; Li et al., 2009; 2014), as illustrated in Eq. (3):

$$\sigma_{eff} = \sigma_c - \alpha_{(P_p,\sigma_c)} \cdot P_p \tag{3}$$

The $\alpha_{(P_p,\sigma_c)}$ is a pore pressure/confining stress dependent (named as "stress dependent" thereafter) effective stress coefficient. In this paper, all of the α used thereafter represents $\alpha_{(P_p,\sigma_c)}$.

In this study, the stress dependency of elastic modulus of clay will be incorporated into the CSM to depict the complicate relationship between α, σ_c and P_p. We discretized the materials (sand grains and clay) into several thin rings to calculate the stress dependent elastic moduli of clay at different radial distance r to the center of pore. Using this proposed Discretized Clay Shell Model (DCSM) and the response-surface method proposed by Box and Draper (1987), the variation of α with pore pressure P_p and confining stress σ_c can be determined without much difficulties. The experimental data of stress dependent elastic moduli of kaolinite power (Unconsolidation) documented by Mondol et al. (2008), as well as two more synthetic clay with different stress sensitive of elastic modulus, were incorporated into the DCSM to evaluate the influence of clay fraction F_c and stress dependency of elastic modulus on α.

Moreover, we provided a synthetic case which the variations of pore pressure P_p and confining stress σ_c at different burial depth of clayey sandstone reservoirs were given. The stress dependent effective stress coefficient α was determined using the proposed DCSM. The effective stress, as well as the permeability, can thus been calculated. The importance of relation between pore pressure P_p, confining stress σ_c, and stress dependent effective stress coefficient α to the determination of effective stress and permeability will be illustrated accordingly.

2 Discretized Clay Shell Model (DCSM) and stress dependent effective stress coefficient α

2.1 Stress independent effective stress coefficient α of permeability

If the effective stress coefficient α is stress independent (independent of confining stress σ_c and pore pressure P_p), Eq. (1) can be used to predict the effective stress. Under this assumption,

Bernabe (1987) proposed Eq. (4) to calculate the effective stress coefficient α of permeability via the permeability measurement under different pore pressure P_p and confining stress σ_c:

$$\alpha = -\frac{\left(\frac{\partial k}{\partial P_p}\right)_{\sigma_c}}{\left(\frac{\partial k}{\partial \sigma_c}\right)_{P_p}} \quad (4)$$

where $\left(\frac{\partial k}{\partial P_p}\right)_{\sigma_c}$ and $\left(\frac{\partial k}{\partial \sigma_c}\right)_{P_p}$ are partial derivative of permeability k to pore pressure P_p and confining stress σ_c, respectively. Based on the Hagen-Poiseuille equation and Darcy's law, the permeability k of along a cylindrical tube can be expressed as (e.g. Civan et al., 2011; Cao et al., 2016):

$$k = \frac{r_p^4}{8r_g^2} \quad (5)$$

where the r_p and r_g are the radius of pore and grains (Fig. 1a), respectively. If the r_g assumed as constant (Eulerian permeability), and insert Eq. (5) into Eq. (4), the effective stress coefficient α can be calculated using following equation:

$$\alpha = -\frac{\left(\frac{\partial r_p}{\partial P_p}\right)_{\sigma_c}}{\left(\frac{\partial r_p}{\partial \sigma_c}\right)_{P_p}} \quad (6)$$

That is, the effective stress coefficient α of permeability can be determined based on the pore radius variations. The relations between the pore radius r_p, σ_c and P_p incorporate in CSM will be introduced in the following section.

2.2 Clay Shell Model (CSM) of Clayey sandstones

CSM conceptualized the clayey sandstones into a system with hollow cylinder pore in grains coating by clay (Fig. 1a). If the variations of r_p with σ_c and P_p can be evaluated, the α can be obtained using Eq. (6). Based on plain strain assumption (Fig. 1b) and axial symmetry, the

146 calculation is simply a 1-D problem. The only component related to r_p is the radial displacement
147 vector $u_{(r)}$ along radius in cylindrical polar coordinate (Fig. 1b). The derivation of the relationship
148 between $u_{(r)}$ and stress condition (σ_c and P_p) can be found in text book of elastic theory (e.g.,
149 Sokolnikoff, 1956; Jaeger and Cook, 1979). In this paper, the basic idea was introduced briefly to
150 better illustrate our proposed model in Section 2.3.

151 For a hollow tube model, the radial displacement $u_{(r)}$ at radial location r from the center of
152 the tube to a specific point can be expressed as:

153 $$u_{(r)} = Ar + \frac{B}{r} \tag{7}$$

154 if the material around the radial location r is homogeneous (the tube wall in Fig.1 composed of only
155 one material). The A and B are parameters related to elastic moduli of the material composed of
156 the tube wall. To solve A and B, the relation between radial stress σ_r and u is required as follows
157 (Sokolnikoff, 1956):

158 $$(\lambda + 2\mu)\frac{du_{(r)}}{dr} + \lambda\frac{u_{(r)}}{r} = \sigma_r \tag{8}$$

159 where λ and μ are Lamé constant and shear modulus. The radial stress σ_r at $r = r_p$ and $r = r_g$
160 are P_p and σ_c. Therefore,

161 $$(\lambda + 2\mu)(A - \frac{B}{r_p^2}) + \lambda(A + \frac{B}{r_p^2}) = P_p \tag{9}$$

162 $$(\lambda + 2\mu)(A - \frac{B}{r_g^2}) + \lambda(A + \frac{B}{r_g^2}) = \sigma_c \tag{10}$$

163 The two unknowns A and B can be solved via Eqs. (9) and (10). The radial displacement
164 when $r = r_p$ (=variation of pore radius) can be expressed by Eq. (11):

165 $$u_p = Ar_p + \frac{B}{r_p} \tag{11}$$

where u_p denotes the displacement of pore radius. The u_p can be used to calculate the variation of pore radius r_p caused by σ_c and P_p, and determine the effective stress coefficient α using Eq. (6). Notability, the α is stress independent which is a big assumption of CSM.

If the tube wall is composed of two materials (clay and grains, CSM in Fig. 1a), the parameters A and B for domains of clay and grains will be different. We use the A_c and B_c representing the parameters for clay domain and A_g and B_g for grain domain. Two more constrain conditions, i.e., radial stress σ_r and displacement u are identical on the boundary of clay and grains domains when $r = r_c$, together with two boundary conditions were used to solve the four unknowns. The solved four parameters (A_c and B_c; A_g and B_g) are function of clay fraction F_c, porosity ϕ, Poisson's ratio υ, and shear modulus ratio γ (defined in Eq. (12)), which can be found in Al-Wardy and Zimmerman (2004).

$$\gamma = \frac{\mu_g}{\mu_c} \tag{12}$$

The μ_g and μ_c are shear modulus of grains and shear modulus of clay, respectively (see Fig. 1a). Fig. 2 shows the predicted α of sandstones with clay fraction F_c from 0 to 0.3 using CSM (Al-Wardy and Zimmerman, 2004). Five curves represent the different α when γ (ratio of shear modulus between grains and clay) equal to 1, 5, 10, 25, 50. The porosity ϕ of the clayey sandstones equals to 0.2. The Poisson's ratio υ of clay and grains equals to 0.25.

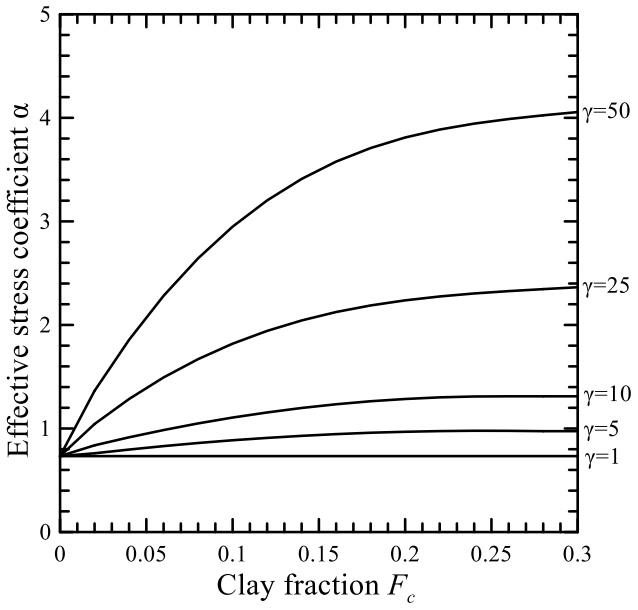

Figure 2. The predicted α of clayey sandstones using CSM with porosity $\phi = 0.2$, under different clay fraction F_c and shear modulus ratio γ. The Poisson's ratio $\upsilon = 0.25$ for grains and clay. (modified from Al-Wardy and Zimmerman, 2004)

When $\gamma = 1$ or $F_c = 0$, which represent a clean sandstone, the $\alpha = 0.713$. This value can be obtained analytically (Al-Wardy and Zimmerman, 2004). Generally, the effective stress coefficient α increases with increasing γ (decreases the shear modulus of clay while the shear modulus of grains is remains unchanged) and clay fraction F_c. Since the elastic moduli of clay and grains are assumed as stress-independent in CSM, the effective stress coefficient α is a constant when the F_c and γ are fixed and will not vary with changing confining stress σ_c and pore pressure P_p.

As aforementioned, the elastic moduli of clay are frequently stress-dependent (e.g. Mondol et al., 2008). The elastic moduli of clay at different r should not be identical since the radial stress σ_r is function of radial position r (Eq. (8) and Fig. 3).

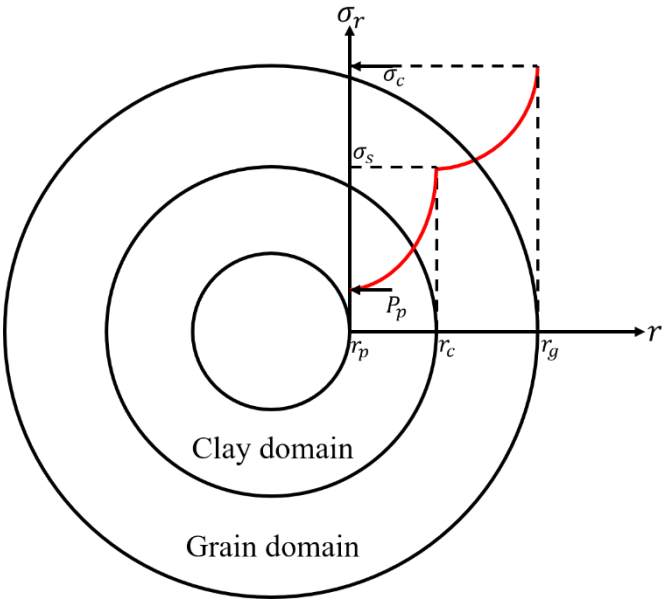

Figure 3. The radial stress distribution along the radial direction of the CSM. The gradient of radial stress for clay and grain is different for their elastic moduli are different. The two boundary stresses are P_p when $r = r_p$ and σ_c when $r = r_g$, respectively. σ_s is the radial stress when $r = r_g$. The radial stress is continuous on the boundary of clay and grains.

2.3 Discretized Clay Shell Model (DCSM)

According to Fig. 3, radial stress σ_r is varied with location. The elastic moduli of material at different location will be different if the elastic moduli is stress dependent. To accounts for the issue of elastic moduli heterogeneity, we discretized the clay and sand grain domains in Fig. 3 into numerous thin rings as show in Fig. 4. The r_p is the pore radius. The r_i (i=1~N) represents the outer radius of i-th ring. Here, the r_N (i = N) is equivalent to the outer boundary of grain domain r_g defined in previous sections. The Poisson's ratio and shear modulus of i-th ring denoted by ν_i and μ_i.

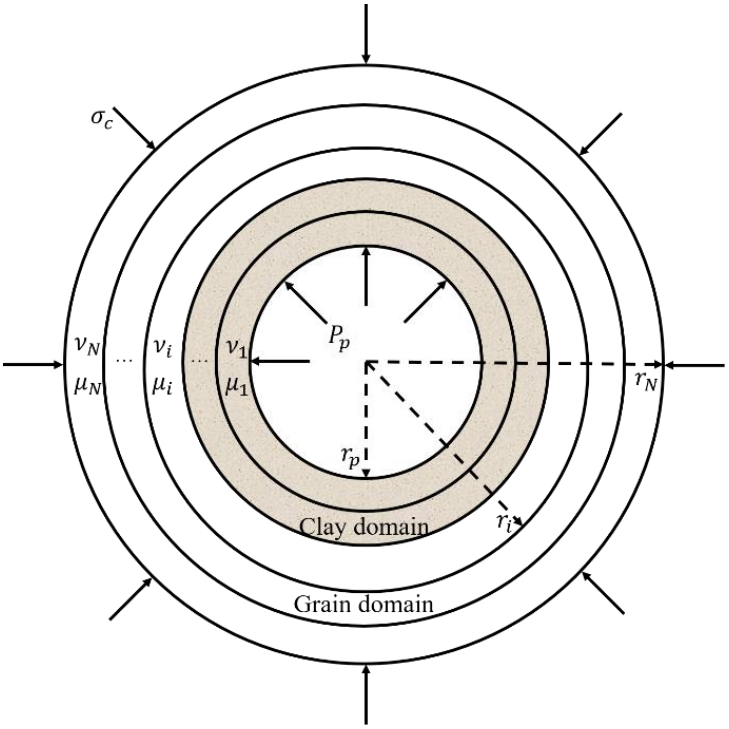

Figure 4. The Discretized Clay Shell Model (DCSM). There are N rings with different elastic moduli ν_i and μ_i. The r_p is the pore radius. The r_i is the outer boundary of the *i*-th ring.

The parameters of A and B in Eq. (7) for each ring are different and can be denoted by A_i and B_i. Therefore, totally 2N unknowns need to be solved. As aforementioned, there are 4 unknowns (A_c and B_c; A_g and B_g) were solved for CSM via 2 boundary conditions (pore pressure and confining pressure applied on the inner boundary of clay domain and outer boundary of grain domain) and 2 constrain conditions (radial stress and displacement are identical on the boundary of clay and grains domains). Likewise, there are two boundary conditions and 2N-2 constrain conditions (radial stress and displacement on boundary of *i*-th ring and the (*i*+1)-th ring) in DCSM. Totally 2N equations were available to solve the 2N unknowns (A_i and B_i, $i = 1\sim$N). The displacement of pore radius can be calculated by Eq. (11) with the determined parameters (A_1 and B_1) for the 1st ring.

227 Now the proposed DCSM can be used to calculate the displacement of pore radius u_p under
228 different σ_c and P_p, since the radial stress dependent moduli of the clay domain will be function of
229 both of them. However, Eq. (6) cannot be used directly for the effective stress coefficient $\alpha_{(P_p,\sigma_c)}$ is
230 not a constant anymore. The response-surface method proposed by Box and Draper (1987) was used
231 to determine the stress dependent effective stress coefficient for permeability under different σ_c and
232 P_p, which will be introduced in next section.

233

234 2.4 Response surface method: determining the stress dependent effective stress coefficient $\alpha_{(P_p,\sigma_c)}$

235 The response surface method proposed by Box and Draper (1987) was used in this study to
236 determine the effective stress coefficient $\alpha_{(\sigma_c,P_p)}$. Based on Eq. (5), we can use the variations of the
237 pore radius r_p (can be calculated by displacement of pore radius u_p determined by the proposed
238 DCSM) due to changing of σ_c and P_p to represent the stress dependent permeability $k_{(P_p,\sigma_c)}$. The
239 relation of pore radius r_p to the confining stress σ_c and pore pressure P_p can be depicted as a
240 response surface and illustrated in Fig. 5a. Fig. 5b is a horizontal projection of Fig. 5a. The contours
241 in Fig. 5b are iso-r_p curves where the pore radius under different confining stress and pore pressure
242 are identical. Based on Eq. (5), the iso-r_p curves in Fig. 5b are iso-*k* curves, too. If the effective
243 stress principle is valid, the iso-*k* curve can also be the iso-σ_{eff} curves.

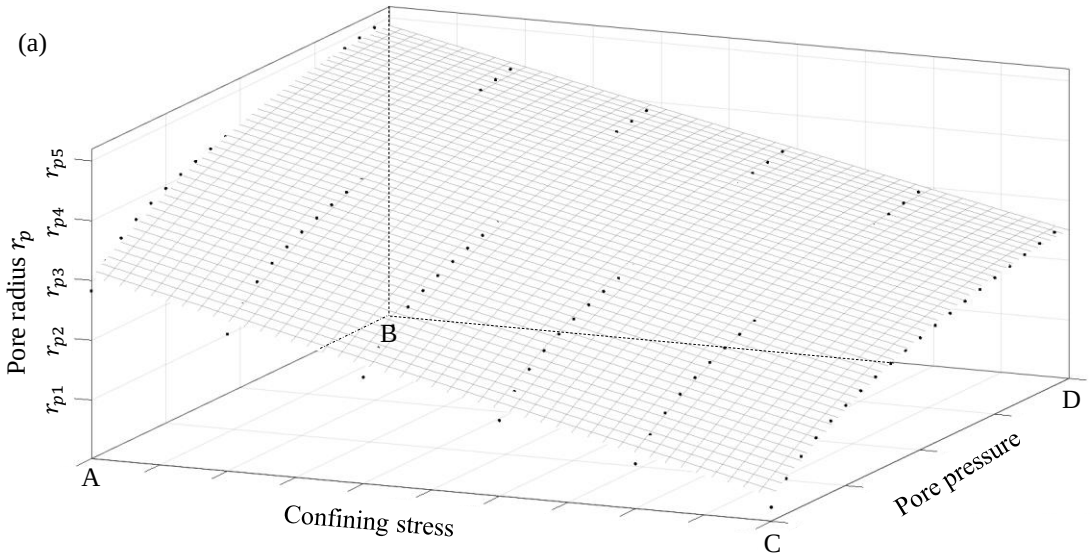

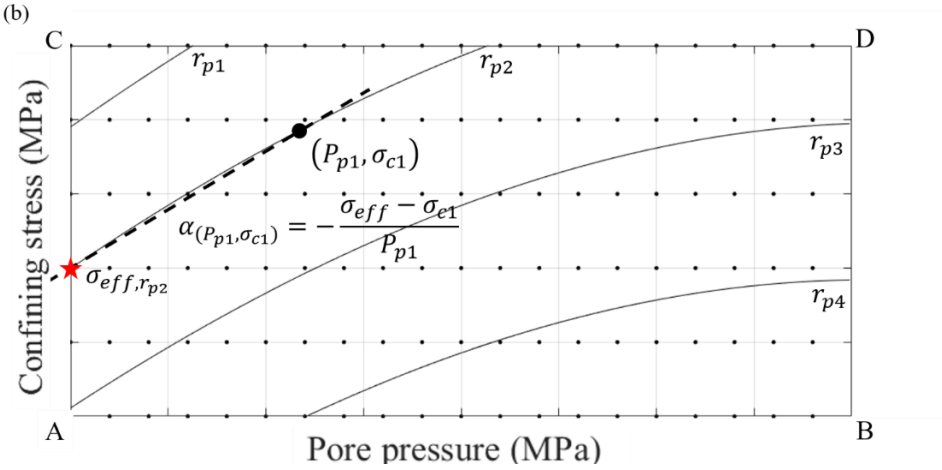

Figure 5. Response surface method for determining the effective stress coefficient α. (**a**) Variations of pore radius versus changing of confining stress and pore pressure; (**b**) The contours of pore radius under different confining stress and pore pressure, each curve represents iso-r_p curve. The α will be the secant slope between red star and black circle.

If the effectives stress coefficient α is a constant (independent of σ_c and P_p), the surface in Fig. 5a should be a plane. The iso-r_p curves in Fig. 5b will be straight lines. According to Eq. (1), the effective stress will equal to confining stress when $P_p = 0$. That is, the intercepts of the iso-r_p

curves and the confining stress axis are effective stress, such as the star marked on 5b. The slope of iso-r_p lines actually are effective stress coefficient α according to Eq. (1). The α would also be the same by using Eq. (6) if the surface in Fig. 5a is a plane.

If the effectives stress coefficient α is stress dependent, the slopes of iso-r_p curves in Fig. 5b will vary with pore pressure and confining stress. According to Eq. (3), the effective stress coefficient $\alpha_{(P_{p1},\sigma_{c1})}$ when the confining stress and the pore pressure equal to σ_{c1} and P_{p1} (circle on Fig. 5b) can be determined as follows:

$$\alpha_{(P_{p1},\sigma_{c1})} = -\frac{\sigma_{eff}-\sigma_{c1}}{P_{p1}} \quad (13)$$

since the iso-r_p curves represent the iso-σ_{eff} curves and the y-axis of stars in Fig. 5b represents the σ_{eff}. That is, the stress dependent effectives stress coefficient $\alpha_{(P_p,\sigma_c)}$ is the secant slope of dash line connecting star (0, $\sigma_{eff,r_{p2}}$) and circle (P_{p1}, σ_{c1}) marked on Fig. 5b.

3 Geometry and material properties used in DCSM

3.1 Geometry and boundary conditions (confining stress and pore pressure)

The initial outer boundary of grain domain r_g=25.82 μm and inner boundary of clay domain (pore radius) r_p=10.00μm to make the porosity ϕ equals to 0.2 which is identical to the ones selected by Al-Wardy and Zimmerman (2004) for CSM. The clay and grain domains were divided into 1000 and 100 rings, respectively, for evaluating the radial stress and elastic moduli heterogeneity.

Several combinations of confining stress σ_c and pore pressure P_p were selected. The σ_c and P_p was both designed to increase from 2MPa to 50MPa by 2MPa of intervals.

3.2 Stress dependent elastic moduli of clay

Mondol et al. (2008) show that elastic moduli of clay minerals are stress dependent via the measurement of the density, P-wave and S-wave velocities of kaolinite saturated in brine and subjected to confining stress. They found the density of kaolinite increased from 2.20(g/cm^3) to 2.52(g/cm^3), P-wave velocities increased from 1,697$(\mathrm{m/s})$ to 2,470$(\mathrm{m/s})$, and S-wave velocities increased from 535$(\mathrm{m/s})$ to 1,014$(\mathrm{m/s})$ when the confining stress increasing from 5MPa to 50MPa. According to experimental results from Mondol et al. (2008), the shear modulus of kaolinite under confining stress from 5MPa to 50MPa can be determined as from 0.63GPa to 2.74GPa. The shear modulus of clay μ_c (GPa) at different location, which is essential input parameter of our DCSM, under different confining stress (radial stress σ_r (GPa) in our DCSM) can be evaluated using Eq. (14). This equation was obtained via curve fitting of the testing results of Mondol et al. (2008).

$$\mu_c = -0.92 \times 10^2 \cdot \sigma_r^2 + 9.2 \times 10^1 \cdot \sigma_r + 4.65 \times 10^{-1} \quad 0 \le \sigma_r \le 0.05\mathrm{GPa} \tag{14a}$$

$$\mu_c = \mu_{c,max} \qquad \sigma_r > 0.05\mathrm{GPa} \tag{14b}$$

In Eq. (14), $\mu_{c,max}$ is 2.76 GPa (Substitute $\sigma_r = 0.05$ GPa into Eq. (14a)) which representing the maximum value of shear modulus of clay. When $\sigma_r = 0$ GPa, a minimum shear modulus of clay ($\mu_{c,min}$) will be determined as 0.46GPa using Eq. (14a). The stress dependent shear modulus documented by Mondol et al. (2008) and the curve fitting result was shown in Fig. 6 (circles and dashed line, respectively). The determined Poisson's ratio υ of clay is ranging from 0.44 to 0.39 based on the testing results of Mondol et al. (2008). In this study, the Poisson's ratio of clay was set to be 0.25, which is identical to the one used in the simulation of CSM (Al-Wardy and Zimmerman, 2004) for comparison.

3.3 Elastic moduli of grains

In this study, we assume the elastic moduli of sand grains is stress independent. To compare our result to CSM (Fig. 2), the shear modulus of grains μ_g is 23.2GPa (illustrated in Fig. 6 together with the one of clay, μ_c) which is 50 times larger than the minimum shear modulus of clay $\mu_{c,min}$. That is, the shear modulus ratio $\gamma = 50$ when the radial stress equal to zero. The Poisson's ratio of grains ν_g equals to 0.25, which is also identical to the one of CSM.

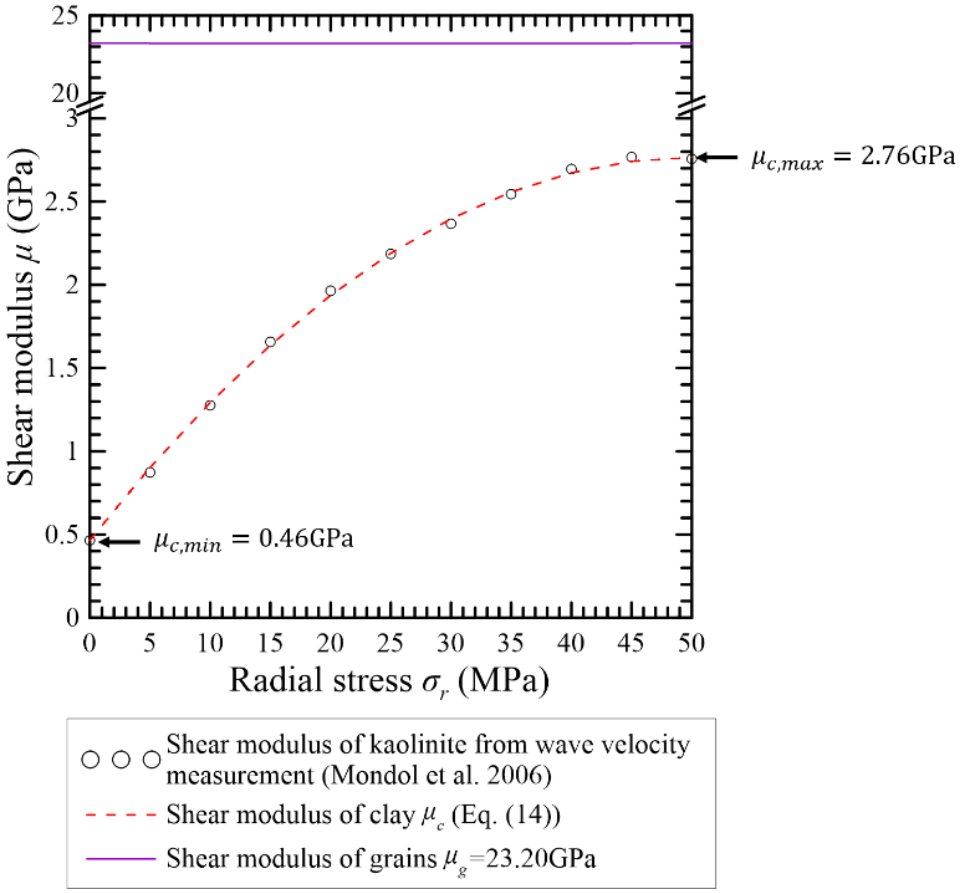

Figure 6. Stress dependent shear modulus of clay. Circles denote the shear modulus of kaolinite calculated from wave measurement (Mondol et al., 2008). Dash red line denotes the stress dependent shear modulus of clay (μ_c) using curve fitting (Eq. (14)). Purple solid line denotes the shear modulus of grains (μ_g) which is stress independent (a constant, equals to 23.2GPa).

312 The shear modulus of each ring of clay domain was determined via a trial and error scheme.
313 Initially, the shear modulus of each ring in clay domain equals to $\mu_{c,min}$. The DCSM program yields
314 the radial stress distribution, and new shear modulus in clay domain can be determined. The new
315 ones was inserted back into DCSM program to calculate the radial stress again. When the absolute of
316 relative error ($\frac{\text{New shear mudulus-Old shear modulus}}{\text{Old shear modulus}}$) less than 10^{-3}, the shear modulus of each ring of clay
317 domain will be fixed for the calculation of r_p under different σ_c and P_p.
318

319 **4 Results**

320 4.1 Comparison of the α determined by CSM and DCSM (elastic moduli are stress independent)

321 To verify the proposed DCSM, this study compared the α documented by Al-Wardy and
322 Zimmerman (2004) using CSM and the one calculated by the proposed DCSM. The porosity ϕ of
323 clayey sandstone is assumed as 0.2. The Poisson's ratios of clay and grains (ν) are 0.25, the shear
324 modulus of grains μ_g is 23.2GPa. Fig. 7 show the predicted α varied with clay fraction using CSM
325 (dashed lines) and proposed DCSM (circles). For shear modulus ratio γ ($=\frac{\mu_g}{\mu_c}$) equals to 50, the
326 shear modulus of clay μ_c is 0.46GPa. For shear modulus ratio γ equals to 25, the shear modulus of
327 clay μ_c is 0.92GPa. The comparison shows the DCSM yields identical results of α predicted by
328 CSM when the elastic moduli of clay assumed as stress-independent.
329

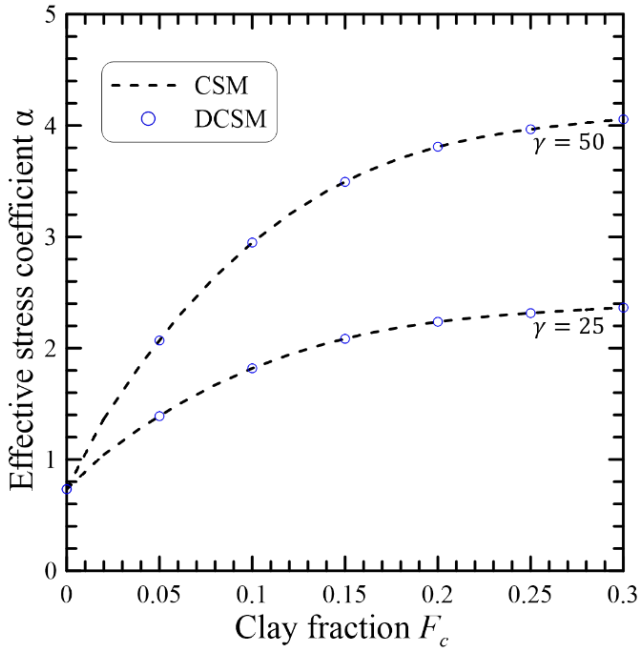

Figure 7. Comparison of the α determined by CSM (Clay Shell Model) and the proposed DCSM. The dashed lines represent the effective stress coefficient α predicted by CSM when the shear modulus ratio $\gamma = 25$ and 50 (shown in Fig. 2 previously). The circles are the calculated α using the proposed DCSM. The parameters used are identical to ones used by Al-Wardy and Zimmerman (2004). The $\mu_g = 23.2$GPa. When $\gamma = 25$, $\mu_c = 0.92$GPa. When $\gamma = 50$, $\mu_c = 0.46$GPa.

4.2 Three different stress-dependent shear modulus of clay with different stress sensitivity

To account for the influence of consolidation degree of clay coating on the sand grains on α of clayey sandstones, this study assigned three different stress dependent shear modulus models of clay with different stress sensitivity. Fig. 8a shows the three stress-dependent shear moduli of Clay 1, 2, 3. The maximum shear modulus ($\mu_{c,max}$) of each clay model is 2.76 GPa. Red dashed line is Clay 1, with $\mu_{c,min} = 0.46$GPa. Blue dashed line is Clay 2, with $\mu_{c,min} = 1.26$GPa. Green dashed line is Clay 3, with $\mu_{c,min} = 2.26$GPa. The stress sensitivity of shear modulus decreased from Clay 1 to Clay 3 and this could relate to the consolidation degree of clay filled in the voids of sand grains. Notable, the curve of Clay 1 is identical to the curve shown in Fig. 6, which is the testing results of kaolinite powder from Mondol et al. (2008).

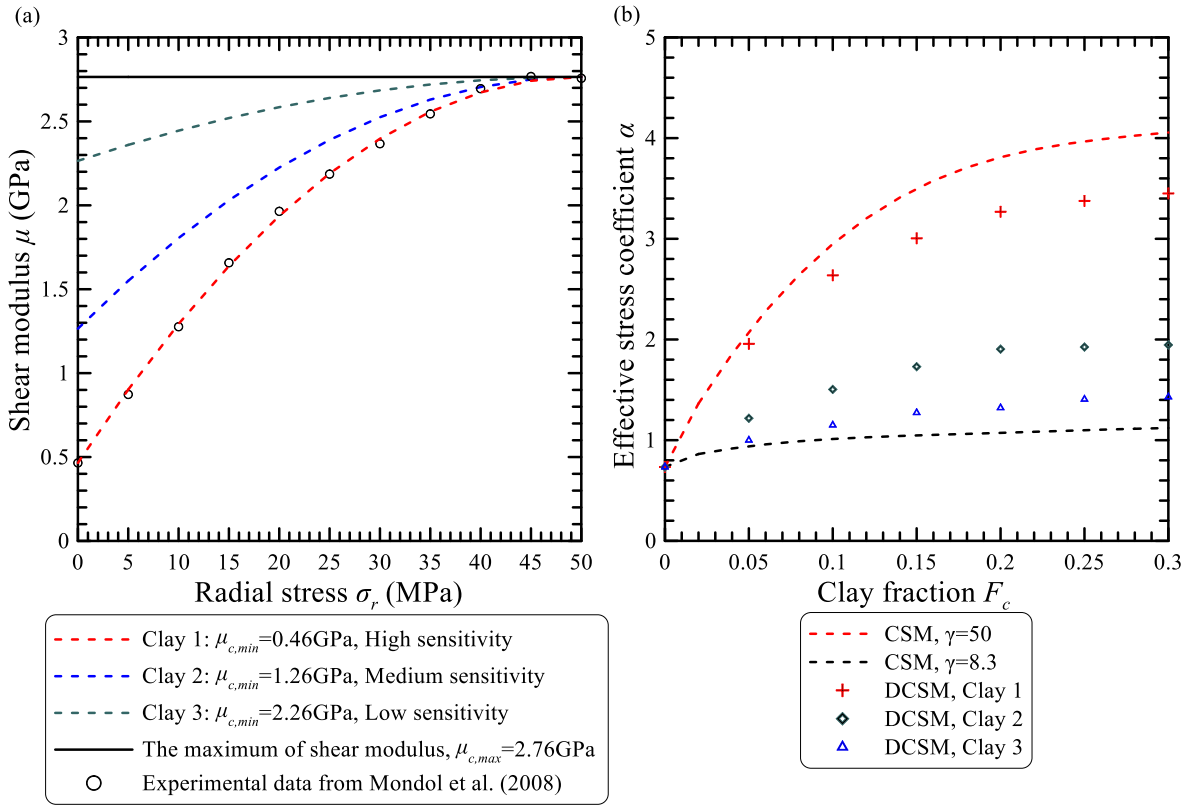

Figure 8. (**a**) Different stress sensitivity of clay shear modulus. The maximum of shear modulus ($\mu_{c,max}$) all maintain at 2.76GPa. The $\mu_{c,min}$ of Clay 1, 2, 3 are 0.46GPa, 1.26GPa, and 2.26GPa, respectively; (**b**) The predicted α with $\sigma_c = 50$MPa and $P_p = 0$ MPa using DCSM assigning shear moduli of Clay 1, 2, 3 with different stress sensitivity. The porosity (ϕ) of clayey sandstone is assumed as 0.2; The shear modulus of grains $\mu_g = 23.20$GPa, the Poisson's ratios of clay and grains (ν) are 0.25. The predicted α for $\gamma = 50$ ($\mu_c = 0.46$ GPa, $\gamma = \frac{\mu_g}{\mu_c}$) and $\gamma = 8.3$ ($\mu_c = 2.76$GPa, $\gamma = \frac{\mu_g}{\mu_c}$) using CSM was provided for comparison.

Fig. 8b depicts the influences of stress dependent shear modulus on α under specific stress condition with $\sigma_c = 50$MPa and $P_p = 0$ MPa. The values of clayey sandstone porosity, the shear modulus of grains, the Poisson's ratios of clay and grains are identical to ones used in Section 4.1. The cross, diamond, and triangle symbols represent the predicted α for Clay 1, 2, and 3, respectively. Again, when $F_c = 0$, the effective stress coefficient α is 0.73 for all clay model which fits the analytical solution of CSM for clean sandstones. When F_c increases from 0 to 0.3, the α

362 increases from 0.73 to 3.45 for Clay 1 (crosses in Fig. 8b). The predicted α for $\gamma = 50$ ($\mu_c =$
363 0.46 GPa) and $\gamma = 8.3$ ($\mu_c = 2.76$ GPa) using CSM was illustrated in dashed lines of Fig. 8b.
364 These two lines are upper and lower bounds of α for Clay 1 since the minimum and maximum
365 shear moduli of Clay 1 are 0.46GPa and 2.76GPa, respectively.

366 When the stress sensitivity of clay shear modulus decreased (Clay 2 and Clay 3), the α
367 decreases accordingly. When F_c equals to 0.3, the α is 1.97 and 1.43 for Clay 2 (diamonds in Fig.
368 8b) and Clay 3 (triangles in Fig. 8b), respectively. These values are smaller than the one for Clay 1
369 (α =3.45 when F_c =0.3). This result indicates that CSM failed to make a precise prediction if the
370 shear modulus of clay is stress dependent with different sensitive. Moreover, the sensitivity of α to
371 the clay fraction will be influenced by the stress dependent model of shear modulus.

372 Please note that the α predicted by DCSM can vary with σ_c and P_p, the boundary conditions
373 used should be specified when comparing with CSM. The influence of different stress condition
374 (combination of σ_c and P_p) will be elaborated further in Section 4.3.

375

376 4.3 Confining stress / pore pressure dependency of α

377 Figure 9 shows the predicted effective stress coefficient α by CSM is irrelevant to the
378 confining stress σ_c and pore pressure P_p. The predicted α equals to 4.05 when the clay fraction
379 $F_c = 0.3$ and $\gamma = 50$, which can be read from Fig. 7.

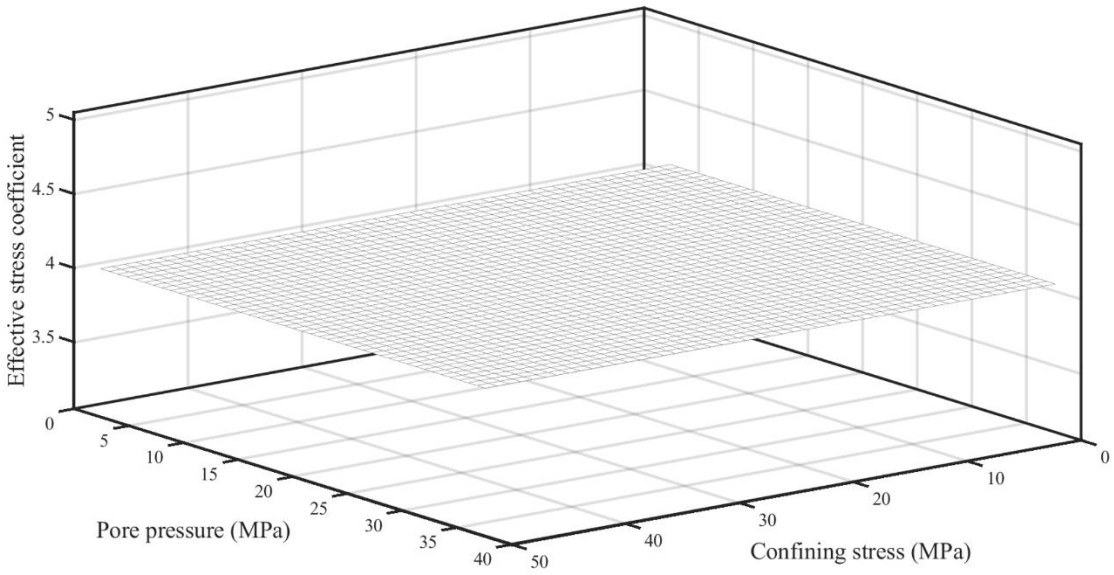

Figure 9. The effective stress coefficient α of clayey sandstones predicted by CSM is pore pressure/confining stress – independent. This plot shows the α equals to 4.05 with clay fraction $F_c = 0.3$ and $\gamma = 50$, which can be read from Fig. 7.

Figure 10a shows the surface depicting the stress dependent effective stress coefficient $\alpha_{(\sigma_c,P_p)}$ versus σ_c and P_p (Clay 1, ϕ=0.2, $F_c = 0.3$, Poisson's ratio of clay and grain υ=0.25). The red vertical planes in Fig. 10a represents the conditions where the pore pressure P_p equals to the confining stress σ_c. This study only focuses on the conditions where P_p lower than σ_c. To visualize the influence of P_p and σ_c on α two dimensionally, Fig. 10b shows the contours of Fig. 10a. Figure 10c shows the relation between $\alpha_{(\sigma_c,P_p)}$ and σ_c when P_p remains unchanged (10, 20, 30 MPa). Figure 10d shows the $\alpha_{(\sigma_c,P_p)}$ under different P_p when σ_c=30, 40, 50 MPa.

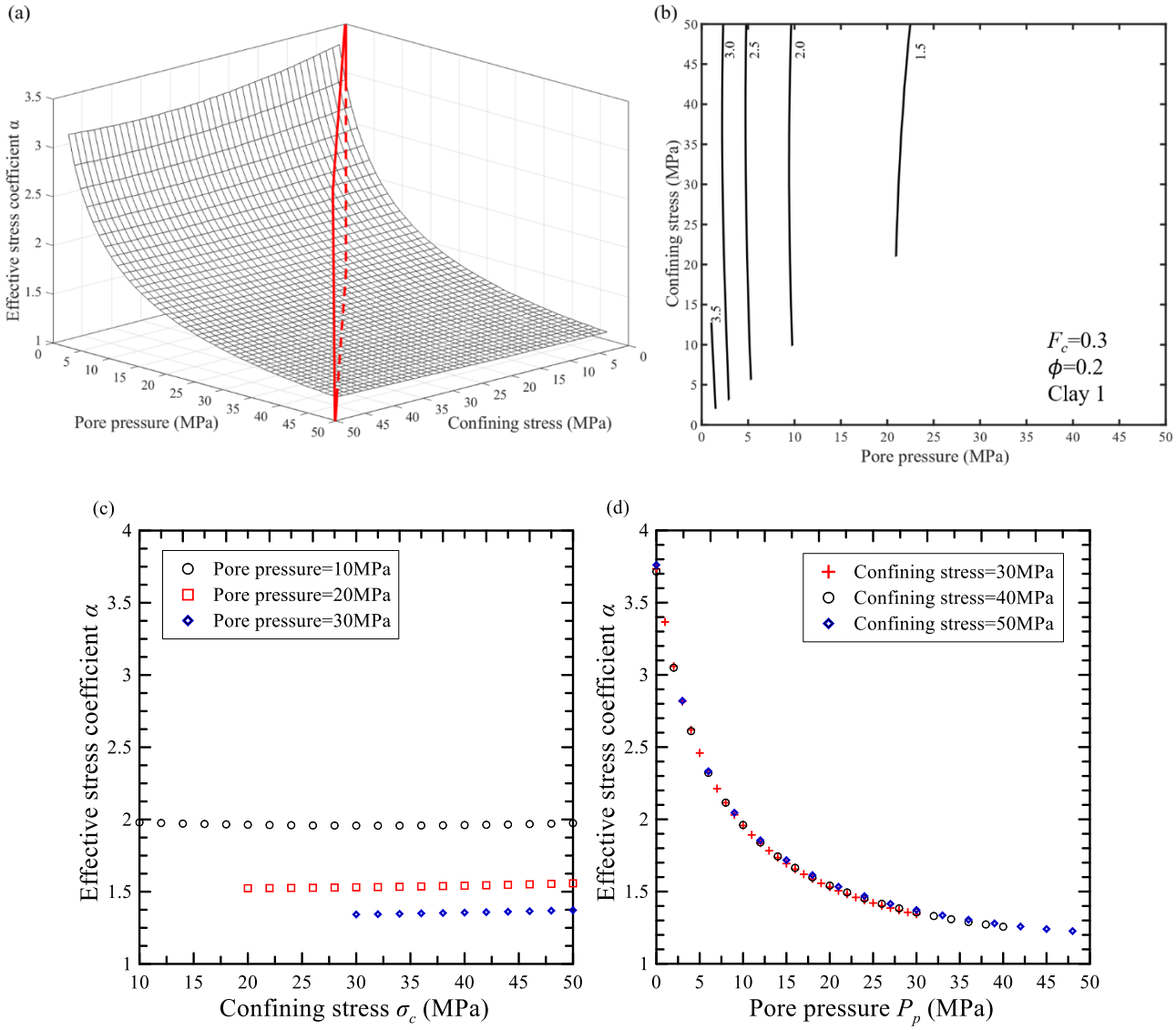

Figure 10. (**a**) The effective stress coefficient α of clayey sandstones (Clay 1, ϕ=0.2, $F_c = 0.3$, Poisson's ratio of clay and grains $\upsilon = 0.25$) predicted by the proposed DCSM is pore pressure/confining stress – dependent. The red vertical planes representing the conditions where the pore pressure P_p equals to the confining stress σ_c; (**b**) The contours of stress coefficient α derived from the surface shown in Fig. 10a; (**c**) The α changes with the confining stress. Black circles, red squares and blue diamonds denote the α changes with the pore pressure when the confining stress is 10MPa, 20MPa, and 30MPa, respectively; (**d**) The α changes with the pore pressure. Red cross and black circles, and blue diamonds denote the α changes with the pore pressure when the confining stress is 30MPa, 40MPa and 50MPa, respectively.

Fig. 10b shows the contours are almost parallel to the y-axis when pore pressure is lower than 15MPa. It indicates the influence of confining stress to the effective stress coefficient α is relatively minor. This can be read from Fig. 10c, too. Figure 10d shows the α is significantly influenced by pore pressure. When the pore pressure is lower than 1MPa, the α can be as high as 3.70 but the α decreases rapidly with increasing pore pressure (Fig. 10d). When pore pressure is larger than 25MPa, the α will be less than 1.5.

4.4 Influence of dominating factors on effective stress coefficient α of clayey sandstones under different combination of confining stress and pore pressure

This section try to illustrate the influence of different factors considered in the proposed DCSM on effective stress coefficient α. Three factors are analyzed: (1) clay fraction F_c; (2) stress dependent shear modulus the clay (Clay l, Clay 2, and Clay 3 in Fig. 8a); and (3) porosity ϕ, under different combination of confining stress σ_c and pore pressure P_p.

4.4.1 Influence of clay fraction on α under different stress condition

Fig. 11a, 11b, and 11c shows the influence of clay fraction (F_c) on α, which the coating material on grain is Clay 1 with ϕ=0.2. It is obviously to find that the α subjected to P_p decreased with decreasing F_c. When $F_c = 0.3$, the range of the α changed from 3.70 to 1.22. However, the range of α changed only from 2.71 to 1.06 when $F_c = 0.1$. Fig. 11a, 11b, 11c finds the influence of confining stress to α is still insignificant when pore pressure is smaller than 20MPa. In all cases, the α are always larger than 1.

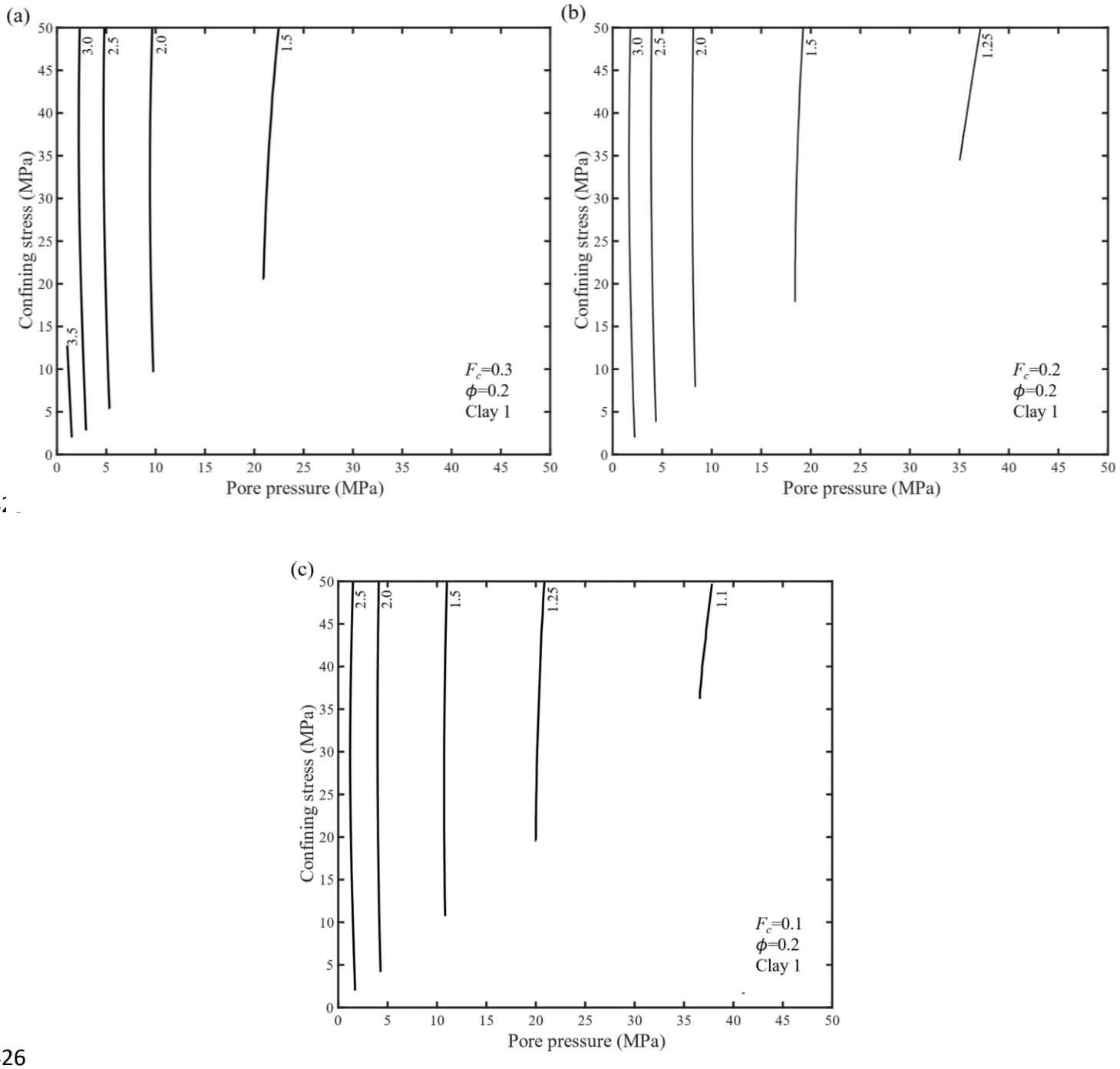

Figure 11. Effective stress coefficient α versus confining stress σ_c and pore pressure P_p of the clayey sandstones for different clay fraction (F_c). The porosity ϕ=0.2, Poisson's ratio of clay and grains $\upsilon = 0.25$, the shear modulus of grains μ_g=23.2GPa. (**a**) $F_c = 0.3$, Clay 1 (refer to Fig. 8a which $\mu_{c,max} = 2.76$GPa, and $\mu_{c,min} = 0.46$GPa); (**b**) $F_c = 0.2$, Clay 1; (**c**) $F_c = 0.1$, Clay 1.

4.4.2 Influence of stress dependent shear modulus of clay on α under different stress condition

The stress dependency of clay materials on the effective stress coefficient α has already been illustrated in Fig. 8. This section try to depict the combined effect of pore pressure, confining stress, and the stress dependency of clay materials (see Fig. 8a), on the effective stress coefficient α. The clay fraction F_c is assumed as 0.3 and the porosity ϕ is 0.2.

The evaluated results are illustrated in Figs. 12a, 12b, 12c. Fig. 12a is the effective stress coefficient for Clay 1 (high stress sensitivity, low consolidation degree). The value of the α changes from 3.70 to 1.22. Fig. 12b is the result for Clay 2 (middle stress sensitivity, middle consolidation degree). It shows the α are smaller than ones of Clay 1. The value of the α changes from 1.97 to 1.21. The material in Fig. 12c is Clay 3 (low stress sensitivity, high consolidation degree). It shows the α is the smallest in all of clay models. The value of the α changes from 1.45 to 1.20. It is obviously to find that the α decreased with increasing consolidation degree of clay. Moreover, the influence of confining stress to α will be affected by the consolidation degree (stress sensitivity) of clay. In Fig. 12a, the contours lines of α approach to vertical straight lines. It implies that the α is not strongly influenced by confining stress. However, the curves in Fig. 12c deviating from the vertical lines and the influence of confining stress becomes significant.

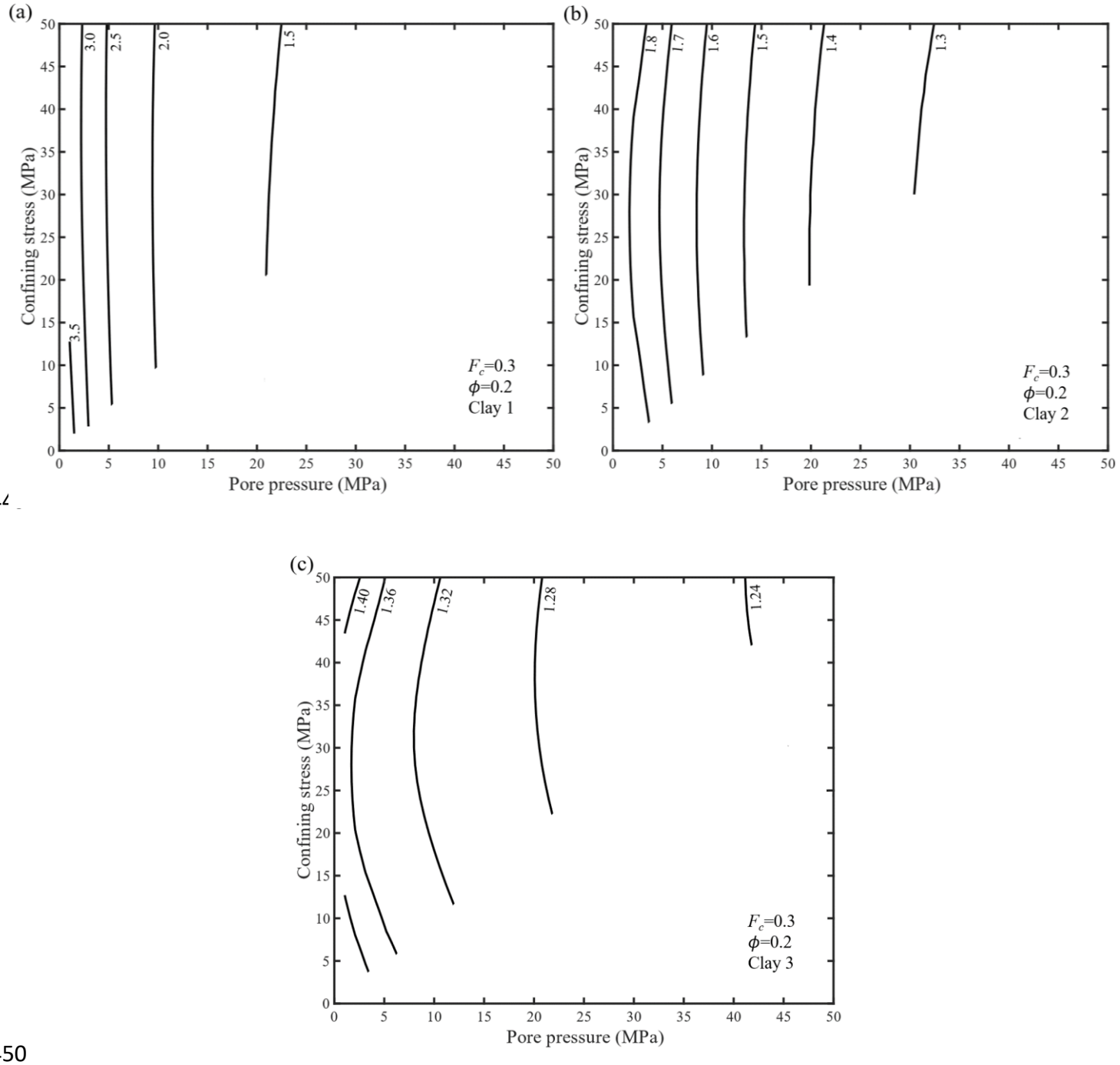

Figure 12. Effective stress coefficient α versus confining stress σ_c and pore pressure P_p of the clayey sandstones for different Clay model (refers to Fig. 8a). The fraction of clay $F_c = 0.3$, the porosity ϕ=0.2, the Poisson's ratio of clay and grains $\upsilon = 0.25$, and the shear modulus of grains μ_g =23.2GPa. (**a**) Clay 1: The $\mu_{c,max} = 2.76\,\mathrm{GPa}$ and $\mu_{c,min} = 0.46\,\mathrm{GPa}$; (**b**) Clay 2: The $\mu_{c,max} = 2.76\,\mathrm{GPa}$ and $\mu_{c,min} = 1.26\,\mathrm{GPa}$.; (**c**) Clay 3: The $\mu_{c,max} = 2.76\,\mathrm{GPa}$ and $\mu_{c,min} =$ 2.26GPa.

457

458 4.4.3 Influence of porosity on α under different stress condition

459 Figure 13a and 13b depict the difference of predicted α of clayey sandstones when the porosity
460 ϕ equals to 0.20 and 0.10, respectively. The clay model is Clay 1 with F_c=0.3. We find that the α
461 increases with decreasing porosity. For ϕ=0.20, the contour values of α ranges from 3.6 to 1.6. For
462 ϕ=0.10, the contour values of α ranges from 5.0 to 1.8. The spacing of contours of α under
463 constant confining stress (parallel to the axis of pore pressure) when ϕ=0.10 is smaller than the ones
464 when ϕ=0.20, indicating a high value of α for porous clayey sandstones and the dropping of α
465 with increasing pore pressure will be significant. Please note that when the clay fraction was fixed,
466 the porosity is related to the pore size directly. The pore radius (r_p) decreases with decreasing
467 porosity ϕ when the outer boundary of grains and clay fraction F_c are fixed. Smaller the pore
468 radius is, the thicker the clay domain is. It results in increasing effective stress coefficient α. It
469 should be note here that the pore volume within the clay is neglected in this study for calculating
470 porosity. That is, the true porosity for all of the synthetic clayey sandstones should be higher.

471

472

473

474

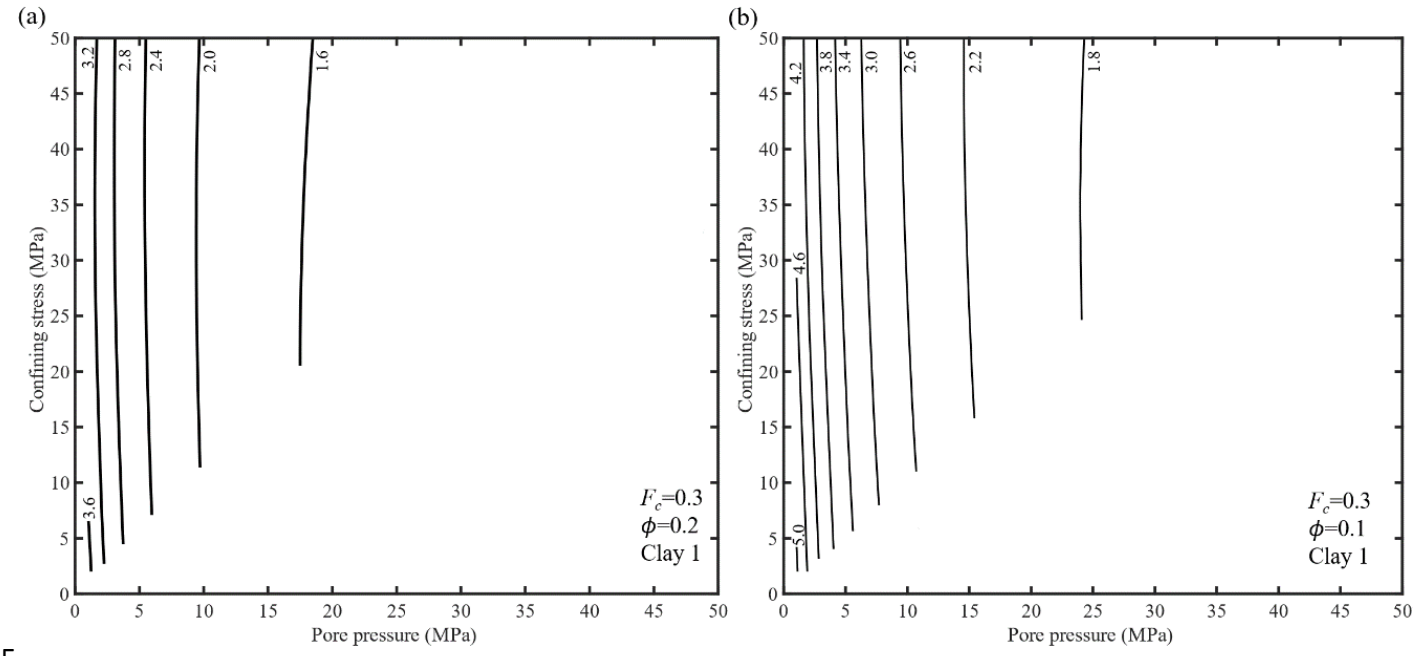

Figure 13. Effective stress coefficient α versus confining stress σ_c and pore pressure P_p of the clayey sandstones for different porosity (ϕ). The Poisson's ratio of clay and grains $\upsilon = 0.25$. The shear modulus of grains μ_g=23.2GPa. The clay fraction $F_c = 0.3$ and the coating clay is Clay 1. (**a**) ϕ=0.2; and (**b**) ϕ=0.10.

5 Discussions

5.1 The controversial measurement results of α for clayey sandstones

5.1.1 Should the α increase or decrease with increasing confining stress?

Quite a lot of experimental results shows the α of clayey sandstones decrease with increasing confining stress (e.g. Siggins and Dewhurst, 2003; Abass, et al., 2009; Dassanayake et al., 2015; Ingraham et al., 2017) when the pore pressure is fixed at relative low pressure (such as 5MPa). On the contrary, Ghabezloo et al. (2009) found the α of limestone (clay coating on the pore wall) increase with increasing confining stress. This controversial results can be explained by the different combination of pore pressure and confining stress. In Fig. 12c, the α will increase with increasing

490 confining stress when the confining stress below certain threshold (~25 MPa when the pore pressure
491 fixed at 5MPa). While the α start to decrease with increasing confining stress when the confining
492 stress goes above this threshold. It is indicated that the coupling effects of pore pressure and
493 confining stress on effective stress coefficient α. The traditional CSM fail to depict this phenomenon.
494

495 5.1.2 Can differential pressure be used to predict α?

496 Some previous studies (e.g., Siggins and Dewhurst, 2003; Abass, et al., 2009) used differential
497 pressure σ_d (confining stress minus pore pressure) to evaluate the effective stress coefficient α.
498 This could oversimplify the combining effect of confining stress and pore pressure on α. Using the
499 calculated contours of α in Fig. 12c as an example, the iso-differential pressure (σ_d) lines (two gray
500 dashed lines) intersected with different contour lines of α, indicating that the differential pressure
501 σ_d could not be a single quantity to evaluate the effective stress coefficient α. However, it is
502 interesting to observed that when the σ_d increased from 5MPa to 45MPa, the variation of α along
503 the iso- differential pressure (σ_d) lines reduced significantly. It indicates that when the differential
504 pressure increased, the simplification to use σ_d for evaluating α could induce minor errors.
505

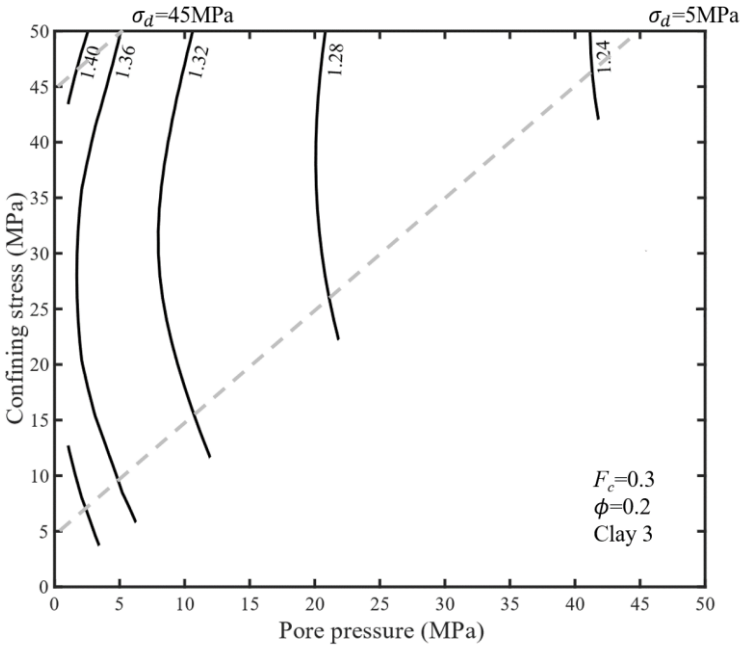

506

507 **Figure 14**. The contours of effective stress coefficient α shown in fig. 12c. The dashed line
508 represent the iso-differential stress σ_d, which are 5MPa and 45MPa, respectively.

509

510 5.1.3 Why the $\alpha < 1$ for some high clay content sandstones?

511 Al-Wardy and Zimmerman (2004) found the α could be up to 5.5 for Stainton sandstone.
512 However, the α measured in some previous studies (e.g. Ingraham et al., 2017) were smaller than 1
513 even the clay fraction approach to 20%. The quantitative evaluation of clay content could be an
514 arguable point. Al-Wardy and Zimmerman (2004) use SEM to identify the clay fraction but the Laser
515 Particle Size Analyzer (LPSA) was used by Ingraham et al. (2017). The SEM image can
516 appropriately evaluate the content of clay coating on the pore wall. However, the clay content
517 characterized by the LPSA cannot guarantee the presence of clay is coated on the pore wall. We
518 suspect the high clay content identified by LPSA could include the grains contain clay mineral,
519 together with the clay filled within the pores (which should be used to evaluate the clay fraction F_c
520 of CSM and DCSM). That is, the clay fraction (parameters of CSM and DCSM) of the clayey
521 sandstones which documented by the papers showing $\alpha < 1$ could be lower than expected. It has

already been indicated that the predicted effective stress coefficient α via CSM could be lower than 1 when the clay fraction is low enough (Fig. 2). Our DCSM predicted α of clayey sandstones below 1 as well (Fig. 15) if the clay fraction is low enough (F_c=0.05) and high consolidation degree (Clay 3, high value and low stress sensitivity of clay shear modulus) clay filled within the pores.

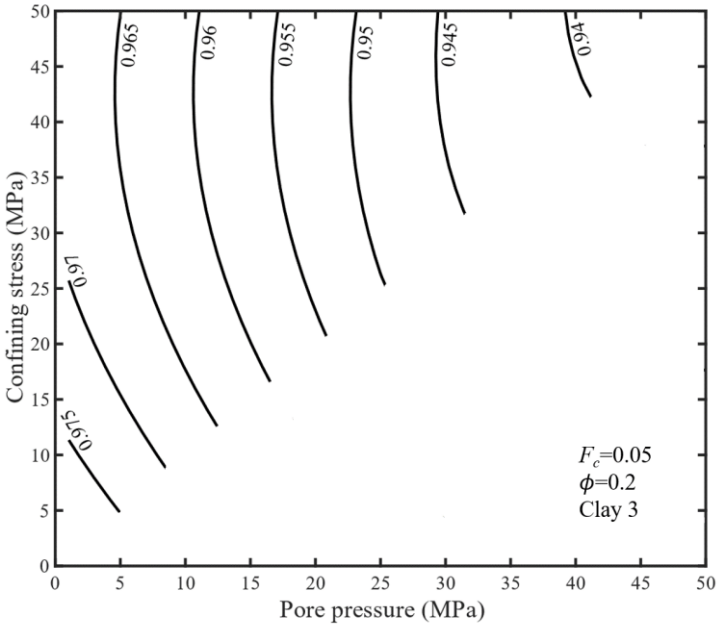

Figure 15. The effective stress coefficient α is always below 1 when $F_c = 0.05$ (low clay fraction) and Clay 3 (high consolidation degree with low stress sensitivity of clay shear modulus which $\mu_{c,max} = 2.76$GPa and $\mu_{c,min} = 2.26$GPa; Fig. 8a) was selected. The porosity of clayey sandstone ϕ=0.2; Poisson's ratio of clay and grains $\upsilon = 0.25$; the shear modulus of grains μ_g=23.2GPa.

The micro cracks within the samples could be another influential factors on the high variability of the measured α. Li et al (2009) measured the effective stress coefficient α for permeability of 23 clayey sandstones under different combinations of stress conditions. The results shows α ranged from 1.33 to 0.86. However, some of the α under different σ_c and P_p could as low as 0.3. Li et al (2009) explained the fractures and micro-fractures accounts for the low α. There are many fractures in samples used in Abass et al. (2009), Dassanayake et al. (2015), and Ingraham et al. (2017) who

also found α of clayey sandstones for permeability are smaller than 1.

5.2 A synthetic case to illustrate how the permeability-depth relation can be predicted via DCSM

We used a synthetic clayey sandstone reservoirs to illustrate the influence of σ_c and P_p on the effective stress coefficient and the predicted permeability-depth relation using effective stress. The unit weight of sandstones $\gamma_w = 25$ (kN/m^3). The total vertical burial stress at depth D, which was used to represent the confining stress $\sigma_c (= \gamma_w \times D)$ in this study, can be determined. The pore pressure increase with burial depth and following the hydrostatic line. The total vertical stress (confining stress) and pore pressure distribution can be found in Fig. 16a.

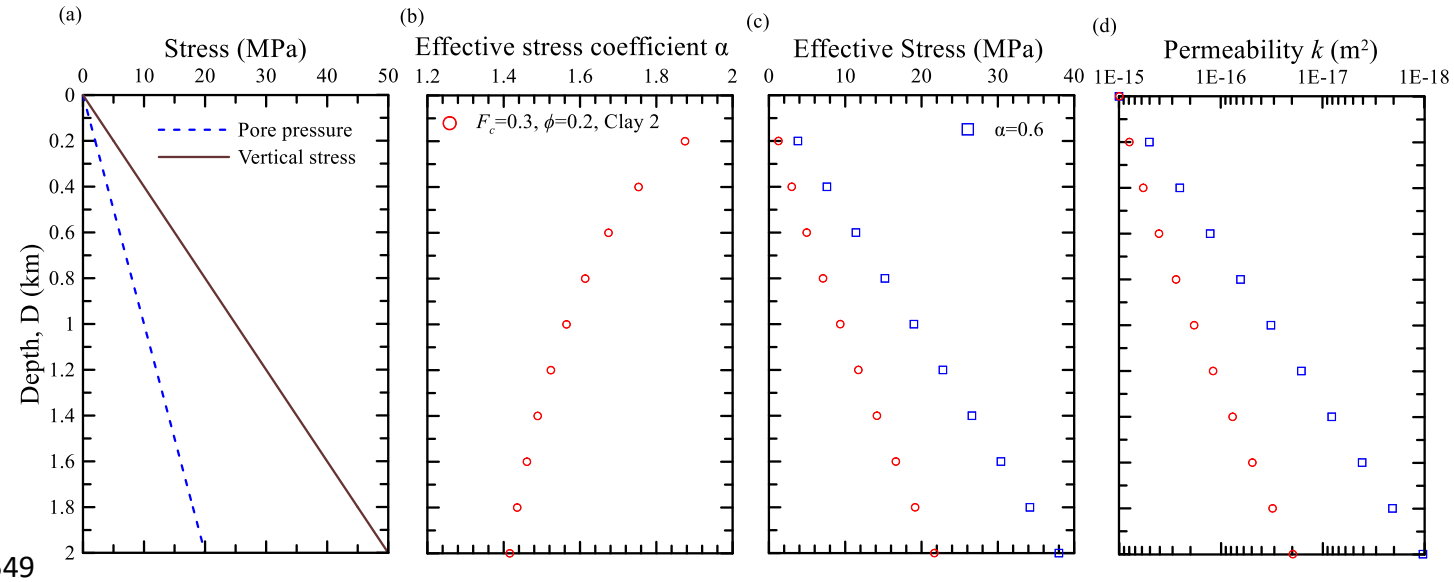

Figure 16. (**a**) Imaged case that excess pore pressure increased with burial depth. (Assume the average of unit weight of formation is 25 kN/m^3); (**b**) The effective stress coefficient α changed with burial depth determined by DCSM ($F_c = 0.3$, $\phi = 0.2$, Clay 2); (**c**) The prediction of effective stress by DCSM, and condition of $\alpha = 0.6$; (**d**) The prediction of permeability based on exponential law proposed by David et al. (1994) (Eq. 15). The stress sensitivity coefficient q=0.018, and permeability at atmosphere pressure k_o= 1 Darcy (10^{-15}m^2).

Based on our proposed DCSM, the α can be determined by pore pressure and the confining stress (vertical stress). The stress dependent model Clay 2 (Fig. 8a) was selected. The porosity (ϕ) of the clayey sandstones is 0.2 and the clay fraction F_c=0.3. Fig. 16b shows the variation of effective stress coefficient α determined by DCSM (dropped from 1.88 to 1.42 from 0.2 km to 2.0 km). The red symbols in Fig. 16c represents the effective stress which calculated by Eq. (3) and the determined α. The blue square symbols are the effective stress assumed $\alpha = 0.6$ (Abass et al., 2009).

This study uses Eq. (15) proposed by David et al. (1994) to model the stress dependent permeability.

$$k = k_o e^{-q(\sigma_{eff} - \sigma_0)} \quad (15)$$

where k_o is permeability at atmosphere pressure, σ_o, which equals to 0.1 MPa, and q is the stress sensitivity coefficient of permeability. We selected q=0.018 which is identical to the parameter for Rothbach sandstone (clay fraction F_c=12%, ϕ=19.9%) in David et al. (1994). The k_o was assumed as 1 Darcy (=10^{-15}m^2).

In Fig. 16d, the variations of permeability *k* at different burial depth are calculated via Eq. (15) using different effective stresses showing in Fig. 16c. Generally, the α determined by DCSM is larger than 1. This makes the predicted effective stress smaller than the one calculated under the condition of α=0.6. It indicates that the *k* will be underestimated if the assumption of α=0.6 is adopted. The maximum discrepancy (at burial depth 2.0km) is about one order of magnitude. It is interesting to note that when the overpressure condition exits, the effective stress α determined by DCSM would be more approached to 1 and the underestimated permeability will be insignificant if we assume $\alpha = 1$.

6 Conclusions

This study modifies Clay Shell Model (CSM) by incorporating the confining stress / pore pressure dependent elastic modulus of clay into discretizing multi-layers clay domain. The proposed

582 Discretized Clay Shell Model (DCSM) determines α under different stress conditions using
583 response surface method. The parametric study and the prediction of permeability-depth relation
584 using synthetic case illustrate the superior features of the proposed DCSM to the traditional CSM.
585 The main findings are summarized as follows:

586 1. The predicted effective stress coefficient α form a concaving upward surface in the pore
587 pressure-confining stress space using DCSM while the traditional CSM yields a constant when the
588 material properties of clay and grain remain unchanged.

589 2. The curvature of the concave surface along the pore pressure axis is smaller (flatter) than the one
590 along the confining stress axis, indicating that the influence of pore pressure on α is stronger than
591 the one of confining stress. When the confining stress keeping as a constant, the predicted α
592 decreased with increasing pore pressure. The decreasing trend is stronger under low pore pressure
593 than the one under high pore pressure. This feature can be observed from the horizontal distance
594 between contour lines increased with increasing pore pressure. It is interesting to note that the
595 predicted α could decrease first with elevated confining stress and start to increase when the
596 confining stress goes up to a threshold value, if the pore pressure remains unchanged. This trend
597 can be observed from the curved contour lines of α.

598 3. The stress dependent shear modulus of clay coating on the grain dominating the variability of the
599 predicted α. When the clay was normally consolidated (Clay 1 model) and the compressibility is
600 large, the value and variability will be large and significant. On the contrary, the predicted α of
601 low stress sensitivity with low compressibility (Clay 3 model) will approach to 1 and the
602 variability is lowest among the three clay model. This result indicates that the effective stress
603 principal proposed by Terzaghi (1943) (i.e., $\alpha = 1$) can be invalidate for young, clayey sandstones.

604 4. Same with the prediction results via CSM, the effective stress coefficient α predicted by the
605 proposed DCSM will increase with increasing clay fraction. The predicted α could be lower than
606 1 for low clay content sandstones under different combination of pore pressure and confining
607 stress. The variability of predicted α under different combination of pore pressure and confining

608 stress using DCSM will increase when the clay fraction increased. That is, the influence of stress
609 dependency of clay shear modulus should not be neglected when the clay fraction is high.
610 5. The effective stress coefficient of clayey sandstones increases with decreasing porosity. The
611 decreased rate of α under low pore pressure will be larger when the porosity of clayey sandstones
612 is lower. This is actually related to the pore size and the thickness of clay domain.
613 6. The applicability for using differential stress σ_d (Difference of confining stress and pore pressure)
614 to predict the effective stress coefficient α depends on the combination of confining stress and
615 pore pressure. It seems that this approach can only be valid under high confining stress, low pore
616 pressure.
617 7. The determination of clay fraction of clayey sandstones should be conducted with caution. From
618 the aspect of DCSM prediction, the SEM approach could superior than the XRD approach for the
619 former one can only include the clay coating on the pore wall. The presence of micro-cracks
620 accounts for the low measured α.
621 8. The synthetic case shows the predicted permeability using the proposed DCSM is significantly
622 larger than the predicted one assuming α=0.6. The maximum discrepancy of predicted
623 permeability at burial depth 2.0 km could be one order of magnitude. However, when overpressure
624 exist, the predicted α will approach to one and the effective stress principle (α=1) assumption
625 will not induce significant error.
626

627 **Acknowledgments**

628 This research was supported by Taiwan Ministry of Science and Technology
629 (MOST108-2638-E-008-001-MY2 and MOST107-2116-M-008-001-MY3). This work was also
630 financially supported by Earthquake-Disaster & Risk Evaluation and Management
631 Center (E-DREaM) from The Featured Areas Research Center Program within the framework of the
632 Higher Education Sprout Project by the Ministry of Education (MOE) in Taiwan. The data published

633 in the literatures used in this study are available through Al-Wardy and Zimmerman (2004), Mondol
634 et al. (2008) and David et al. (1994). All the parameters used in the equations and modeling program
635 are explained in the text. All the data of stress dependent effective stress coefficient with different
636 clay fraction, porosity, and consolidation degree of clay are provided as supporting information.
637

638 **Reference**

639 Abass, H. H., Al-Tahini, A. M., Abousleiman, Y., & Khan, M. R. (2009). *New technique to*
640 *determine Biot coefficient for stress-sensitive dual-porosity reservoirs*. Paper presented at
641 SPE Annual Technical Conference and Exhibition, Society of Petroleum Engineers.
642 https://doi.org/10.2118/124484-MS

643 Al-Wardy, W., & Zimmerman, R. W. (2004). Effective stress law for the permeability of clay-rich
644 sandstones. *Journal of Geophysical Research, 109*(B4).
645 https://doi.org/10.1029/2003JB002836

646 Bernabe, Y. (1987). The effective pressure law for permeability during pore pressure and confining
647 pressure cycling of several crystalline rocks. *Journal of Geophysical Research, 92*(B1),
648 649-657. https://doi.org/10.1029/JB092iB01p00649

649 Berryman, J. G. (1992). Exact effective-stress rules in rock mechanics. *Physical Review A, 46*(6),
650 3307–3311. https://doi.org/10.1103/PhysRevA.46.3307

651 Box, G. P., & Draper, N. P. (1987). *Empirical Model-Building and Response Surfaces*, John Wiley,
652 New York.

653 Breckels, I. M., & van Eekelen, H. A. M. (1982). Relationship between horizontal stress and depth in
654 sedimentary basins. *Journal of Petroleum Technology, 34*, 2191-2198.
655 https://doi.org/10.2118/10336-PA

656 Cao, P., Liu, J., & Leong, Y. K. (2016). General gas permeability model for porous media: bridging
657 the gaps between conventional and unconventional natural gas reservoirs. *Energy & Fuels*,
658 *30*(7), 5492-5505. https://doi.org/10.1021/acs.energyfuels.6b00683

659 Civan, F., Rai, C. S., & Sondergeld, C. H. (2011). Shale-gas permeability and diffusivity inferred by
660 improved formulation of relevant retention and transport mechanisms. *Transport in porous*
661 *media*, *86*(3), 925-944. https://doi.org/10.1007/s11242-010-9665-x

662 Coyner, K. B. (1984). Effects of stress, pore pressure and pore fluid on bulk strain, velocity, and
663 permeability in rocks, (Doctoral dissertation). Massachusetts Institute of Technology,
664 Cambridge, U.K.

665 Cui, X., Bustin, R. M., & Chikatamarla, L. (2007). Adsorption-induced coal swelling and stress:
666 implications for methane production and acid gas sequestration into coal seams. *Journal of*
667 *Geophysical Research: Solid Earth, 112*(B10). https://doi.org/10.1029/2004JB003482

668 Dassanayake, A. B. N.,Fujii, Y., Fukuda, D., & Kodama, J. I. (2015). A new approach to evaluate
669 effective stress coefficient for strength in Kimachi sandstone. *Journal of Petroleum Science*
670 *and Engineering*, *131*, 70-79. https://doi.org/10.1016/j.petrol.2015.04.015

671 David, C., Wong, T. F., Zhu, W., & Zhang, J. (1994). Laboratory measurement of
672 compaction-induced permeability change in porous rocks: implication for the generation and
673 maintenance of pore pressure excess in the crust. *Pure and Applied Geophysics*, *143*(1),
674 425-456. https://doi.org/10.1007/BF00874337

675 Dong, J. J., Hsu, J. Y., Wu, W. J., Shimamoto, T., Hung, J. H., Yeh, E. C., Wu, Y. H., & Sone, H.
676 (2010). Stress-dependence of the permeability and porosity of sandstone and shale from
677 TCDP Hole-A. *International Journal of Rock Mechanics and Mining Sciences*, *47*(7),
678 1141-1157. https://doi.org/10.1016/j.ijrmms.2010.06.019

679 Engelder, T., & Fischer, M. P. (1994). Influence of poroelastic behavior on the magnitude of
680 minimum horizontal stress, S_h in overpressured parts of sedimentary basins. *Geology, 22*(10),
681 949-952. https://doi.org/10.1130/0091-7613(1994)022<0949:IOPBOT>2.3.CO;2

682 Gaarenstroom, L., Tromp, R. A. J., de Jong, M. C., & Brandenburg, A. M. (1993). *Overpressures in*
683 *the central North Sea: Implications for trap integrity and drilling safety*. Paper presented at
684 Geological Society, London, Petroleum Geology Conference series. 4(1), 1305-1313.
685 https://doi.org/10.1144/0041305

686 Gangi, A. F., & Carlson, R. L. (1996). An asperity-deformation model for effective pressure.
687 *Tectonophysics, 256*, 241–251. https://doi.org/10.1016/0040-1951(95)00167-0

688 Ghabezloo, S., Sulem, J., Guedon, S., & Martineau, F. (2009). Effective stress law for the
689 permeability of a limestone. *International Journal of Rock Mechanics and Mining Sciences,*
690 *46*(2), 297-306. https://doi.org/10.1016/j.ijrmms.2008.05.006

691 Ingraham, M. D., Bauer, S. J., Issenm K. A., & Dewers, T. A. (2017). Evolution of permeability and
692 Biot coefficient at high mean stresses in high porosity sandstone. *International Journal of*
693 *Rock Mechanics & Mining Sciences, 96*, 1–10. https://doi.org/10.1016/j.ijrmms.2017.04.004

694 Jaeger, J. C., & Cook N. G. W. (1979). *Fundamentals of Rock Mechanics*, Chapman and Hall, New
695 York.

696 Li, M., Bernabé, Y., Xiao, W. L., Chen, Z. Y., & Liu, Z. Q. (2009). Effective pressure law for
697 permeability of E-bei sandstones. *Journal of Geophysical Research, 114*(B07).
698 https://doi.org/10.1029/2009JB006373

699 Li, M., Xiao, W. L., Bernabé, Y., & Zhao, J. Z. (2014). Nonlinear effective pressure law for
700 permeability. *Journal of Geophysical Research: Solid Earth, 119*, 302-318.
701 https://doi.org/10.1002/2013JB010485

Li, X., Wei, H., Chen, B., Liu, X., Wang, W., & Zhao, X. (2008). *Multi-stage fracturing stimulations improve well performance in tight oil resevoirs of the Changqing Oilfield*. Paper presented at International Petroleum Technology Conference, Kuala Lumpur, Malaysia. https://doi.org/10.2523/IPTC-12303-MS

Mondol, N. H., Jahren, J., Bjørlykke, K., & Brevik, I. (2008). Elastic properties of clay minerals. *The Leading Edge, 27*(6), 758-770. https://doi.org/10.1190/1.2944161

Robin, P. Y. (1973). Note on effective pressure. *Journal of Geophysical Research, 78*, 2434–2437. https://doi.org/10.1029/JB078i014p02434

Siggins, A. F. & Dewhurst, D. N. (2003). Saturation, pore pressure and effective stress from sandstone acoustic properties. *Geophysical Research Letters, 30*(2). https://doi.org/10.1029/2002GL016143

Sokolnikoff, I. S. (1956). *Mathematical Theory of Elasticity*, McGraw-Hill, New York.

Terzaghi, K. (1943). *Theoretical Soil Mechanics*, John Wiley, New York.

Todd, T., & Simmons, G. (1972). Effect of pore pressure on the velocity of compressional waves in low-porosity rocks. *Journal of Geophysical Research, 77*(20), 3731-3743. https://doi.org/10.1029/JB077i020p03731

Walls, J., & Nur, A. (1979). *Pore pressure and confining pressure dependence of permeability in sandstone*. Paper presented at the 7th Formation Evaluation Symposium of the Canadian Well Logging Society.

Zoback, M. D., & Byerlee, J. D. (1975). Permeability and effective stress. *AAPG Bulletin, 59*(1), 154-158. https://doi.org/10.1306/83D91C40-16C7-11D7-8645000102C1865D